- Technical Paper -

MONOTONIC BEHAVIOR OF HIGH STRENGTH CONCRETE WITH BLAST FURNACE SLAG FINE AGGREGATES UNDER FROST ACTION

Muhammad Aboubakar FAROOQ[*1], Yasuhiko SATO[*2], Kyoji NIITANI[*3] and Hiroshi YOKOTA[*4]

ABSTRACT

Freeze-thaw (F-T) test was performed on cylindrical specimens of air-entrained (AE) high strength (HS) concrete with blast furnace slag (BFS) sand compared to AE HS normal concrete. The strain variation inside concrete specimens during the F-T test was recorded, in addition to the dynamic elastic modulus change and mass loss. Thereafter, the static compression tests were performed on concrete specimens with different frost damage levels to examine the change in mechanical properties. No significant degradation in mechanical properties of both concrete was observed due to frost action.

Keywords: Mechanical behavior, High strength concrete, Blast furnace slag fine aggregates, Frost action, Air-entrainment

1. INTRODUCTION

Durability of concrete structures is degraded owing to various mechanical and environmental actions during the service life [1]. Freeze-thaw action, which is among such environmental actions in sub-zero temperature climate regions, poses detrimental effects on the structural performance of concrete structures due to deterioration in mechanical properties of concrete [1,2] because of surface scaling and internal micro-cracking of concrete [3]. In real structures, the frost action is always combined with mechanical loading, which lead to rapid deterioration of the structures. Therefore, the development of durable material, which can resist the mechanical and environmental actions efficiently, is need of the time.

Numerous research work has been conducted to improve the durability of concrete by incorporating admixtures, steel fibers and industrial wastes. Utilization of industrial wastes into concrete helps to protect the environment and conserve the natural resources. Blast furnace slag (BFS) is one of such industrial wastes, which is generated as a by-product during manufacturing of iron. According to statistical report of Nippon Slag Association, over 20 million tons of slag is produced annually and 90% of it is consumed in cement and concrete production [4]. In the recent years, it has been reported that durability related properties of mortar and concrete against various environmental actions can be improved by using ground granulated BFS (GGBFS) as percentage of binder and BFS sand as full amount of fine aggregates [5,6]. Murata et al. (1983) investigated the freeze-thaw resistance of concrete using ground granulated BFS as sand and found improved durability of such concrete [7]. Ayano and Fujii (2014) found improved resistance of concrete with GGBFS and BFS sand against freezing and thawing [8]. However, limited research is available related to elucidation of mechanical properties of such mortar and concrete with BFS fine aggregates. Farooq et al. (2017) reported slightly enhanced fatigue life of mortar with BFS fine aggregates compared to ordinary mortar in air condition [9]. Farooq et al. (2018) examined the mechanical properties of non-air-entrained (non-AE) concrete with BFS fine aggregates subjected to freeze and thaw and found that non-AE BFS concrete showed more compressive strength and Young's modulus and less plastic strain development compared to ordinary AE concrete at different frost damage level [1]. Moreover, the degradation of mechanical properties of AE ordinary concrete was slower compared to non-AE BFS concrete. However, the freeze-thaw cycles (FTC) induced plastic strain and mechanical properties of AE BFS concrete subjected to freeze-thaw cycles is not clarified yet.

Accordingly, the experimental investigation is carried out to study the performance of AE concrete with BFS sand and high early strength cement against freeze-thaw cycles based on FTC induced plastic strain. In addition, the monotonic behavior of AE concrete with BFS sand is also investigated compared to AE HS normal concrete for different frost damage levels.

2. EXPERIMENTAL OUTLINE

2.1 Materials and Specimens Preparation

Cylindrical specimens measuring 100Φ x 200 mm from two types of concrete were casted i.e. BFS concrete and normal (N) concrete. The high early strength Portland cement was used in both types of concrete with air-entraining (AE) agent. Blast furnace slag sand was

*1 Graduate Student, Graduate School of Engineering, Hokkaido University, JCI Student Member
*2 Professor, Department of Civil and Environmental Engineering, Waseda University, JCI Member
*3 Manager R&D, Research Institute, Oriental Shiraishi Corporation, Dr. Env. Sc.
*4 Professor, Faculty of Engineering, Hokkaido University, JCI Member

Table 1 Mix proportions of Normal and BFS concrete

Concrete Type	W/C (%)	AC (%)	s/a (%)	Unit content (kg/m^3)					WRA	Th.	AEA	AFA
				W	C	BFS	CS	G	(C x %)			
N	43	4.5±1	44	158	367	0	786	1012	0.4	-	0.50	-
BFS	43	4.5±1	45	158	367	831	0	1012	0.75	0.04	2.00	2.00

W: water, C: High Early Strength Portland Cement, AC: Air content, s/a: sand to aggregate ratio, BFS: Blast furnace slag sand, CS: crushed sand, G: Gravel, WRA: Water reducing admixture, Th.: Thickener, AEA: Air-entraining agent, AFA: Anti-foaming agent.

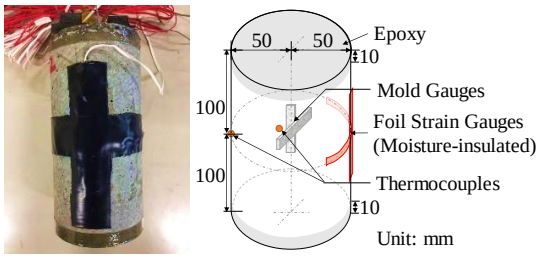

Fig. 1 Description of specimen for freeze-thaw test

used as fine aggregates in BFS concrete, while crushed river sand was used in normal concrete. Table 1 presents the mix proportions for BFS concrete and normal concrete. Prior to casting, the mold gauges of 30 mm gauge length were placed at the center of the cylindrical molds both in axial and lateral directions to measure the strain variations during freeze-thaw test. In addition, the thermocouples were also placed near the center and at the surface of specimen to observe the temperature change during freeze-thaw test. After 36-h of casting, the specimens were demolded followed by curing in water for 28-d at room temperature. Later, the specimens were stored in controlled temperature room at 20°C.

To measure the surface strain variation, the foil strain gauges of 70 mm gauge length were attached to the surface of specimens both in axial and lateral directions. Firstly, the surface of specimens was polished using sand paper and a thin layer of epoxy adhesive was spread at the location of strain gauge and dried for 24-h. After that, the surface of epoxy adhesive was smoothened using the sand paper and strain gauges were attached using the same adhesive and pressed for 24-h for proper attachment. Lastly, a coating layer of moisture proof epoxy was applied over the strain gauges to protect them during freeze-thaw test. Lastly, insulation tape was pasted to further protect the strain gauges from moisture. Moreover, the end surfaces and 1-cm edges of cylinders were coated with epoxy to protect those locations against frost damage for mechanical tests. The configuration of specimen is shown in Fig. 1.

2.2 Freeze-thaw Test Procedure

The freeze-thaw test was performed in accordance with ASTM C-666 type-A [10] in 3% NaCl solution at the age of 5½ months with length of each freeze-thaw cycle of 8-h ranging between +20°C and -25°C. Before starting the freeze-thaw test, the specimens were submerged in 3% NaCl solution for 96-h for proper saturation inside the specimens. Then, the specimens were put inside the rubber tubes filled with 3% NaCl solution such that the top surface of specimen is located around 25mm below the level of solution. The rubber

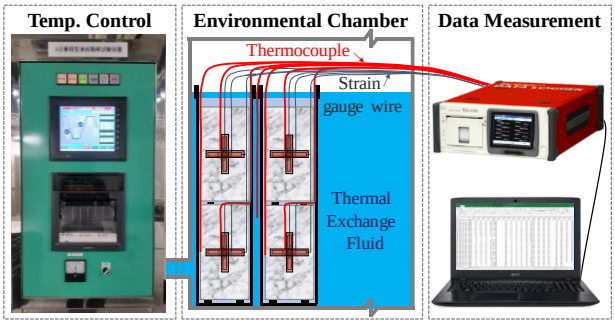

Fig. 2 Freeze-thaw test setup

tubes were then placed in the thermal exchange fluid of the freeze-thaw chamber. The wire of strain gauges and thermocouples were attached to the data logger for recording the data measurement during freeze-thaw test. One thermocouple was also placed in the chamber to record the temperature variation of thermal exchange fluid. Figure 2 represents the set-up of freeze-thaw test.

During the thawing phase at the end of each 15-FTC, the concrete specimens were taken out from F-T chamber and the relative dynamic elastic modulus was measured through ultrasonic pulse wave velocity method by attaching the transmitter and receiver along the longitudinal axis of specimen as shown in Fig. 3. Moreover, the mass loss of the concrete specimens was also determined at the end of each 15-FTC by measuring the weight of oven dried scaled mass collected from the rubber tubes. At the end of thawing phase of 250-FTC and 400-FTC, some specimens were taken out from the freeze-thaw chamber and were stored in frozen condition until the commencement of static compression tests, to avoid any post-FTC curing of frost-damaged concrete.

2.3 Static Compression Test

The uniaxial static compression tests were performed on three specimens of both BFS concrete and normal concrete for each frost damage level i.e. 0-FTC, 250-FTC and 400-FTC at the age of 11 months. The static tests were carried out using displacement-controlled method at the rate of 0.01 mm/sec according to ASTM C39/C39M-14 [11]. The strain measurement was made using axial strain gauges of 60 mm gauge

Fig. 3 Ultrasonic pulse wave velocity setup

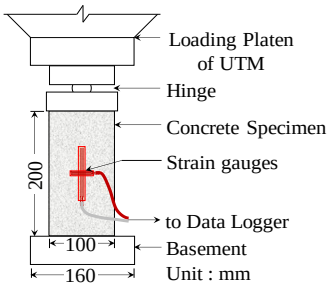

Fig. 4 Loading arrangement of static test

length and lateral strain gauges of 30-mm gauge length. Before attaching strain gauges, the surface of frost damaged concrete specimens was made smooth by grinding and the strain gauges were attached using adhesive. To avoid any eccentricity of applied loading, a hinge was placed in between the loading platen of machine and top surface of specimen. The loading arrangement for static tests is shown in Fig. 4.

After static tests, the static unloading and reloading (U&R) tests were performed on three specimens of each concrete for each damage level to examine the change in mechanical properties. The loading part of each cycle was applied up to different load levels using the same procedure as that of static tests, however, the unloading was done using manual control. After the application of some cycles during static (U&R) test, the specimens were loaded to failure.

3. RESULTS AND DISCUSSION

3.1 Freeze-Thaw Properties

(1) Temperature Variation

The histories of input temperature of FTC and recorded on the surface, at the center of specimens and inside thermal exchange fluid for 225-FTC are shown in Fig. 5. The temperature changes inside the thermal exchange fluid and on the surface of specimen well followed the input temperature. However, the temperature reached at the center of specimens of both concrete was bit behind the input temperature, and the maximum and minimum temperature reached to +15.5±0.5°C and -24.5±0.5°C at the end of each FTC. The similar tendency of temperature change was observed for the whole F-T test.

(2) Relative dynamic elastic modulus and mass loss

The transit time of ultrasonic pulse wave transmitting through the specimens was recorded during the thawing phase at the interval of each 15-FTC and corresponding velocity of wave was determined. The dynamic elastic modulus and relative dynamic elastic modulus (RDEM) of BFS concrete and normal concrete specimens were calculated using Eq. (1) proposed by Ogata H. et al. (2002) [12] and Eq. (2) respectively.

$$E_d = 4.039V_L^2 - 14.438V_L + 20.708 \quad (1)$$

$$RDEM\ (\%) = (E_{dn} / E_{d0}) \times 100 = (t_n / t_0) \times 100 \quad (2)$$

Where,

E_d : dynamic elastic modulus, (GPa)
V_L : velocity of passing ultrasonic wave (km/sec)
E_{dn} : E_d at respective FTC (GPa)
E_{d0} : E_d at start of F-T test (GPa)
t_n : transit time of wave at respective FTC (μ-s)
t_0 : transit time of wave at start of F-T test (μ-s)

The RDEM change and mass change of AE BFS and high strength (HS) normal concrete specimens corresponding to FTC number are shown in Fig. 6, along with the results reported in the past paper [1]. No reduction in RDEM was found during the whole freeze-thaw test in this study, which is because the AE voids in both concrete specimens provided the space to compensate the freezing of the pore water preventing the micro-cracking inside the specimens. However, the amount of scaled mass for AE BFS concrete is slightly more than that of AE HS normal concrete contrary to that of non-AE BFS concrete with ordinary portland cement (OPC) as binder in the previous study [1]. The relationship between RDEM and mass loss is shown in

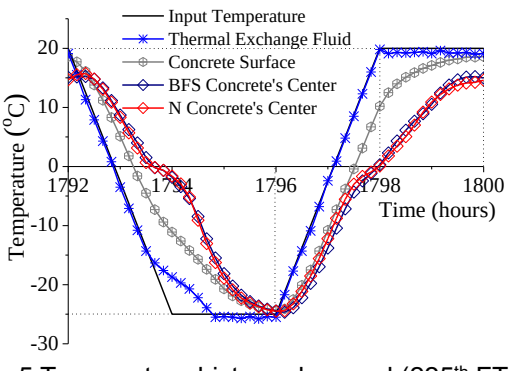

Fig. 5 Temperature history observed (225th FTC)

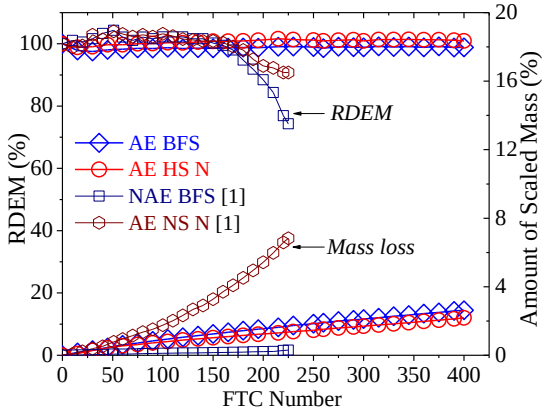

Fig. 6 RDEM change and Mass loss

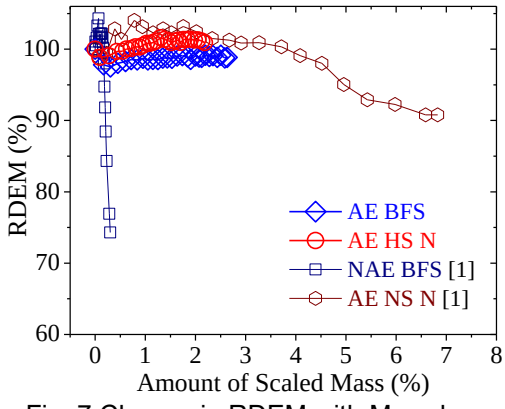

Fig. 7 Change in RDEM with Mass loss

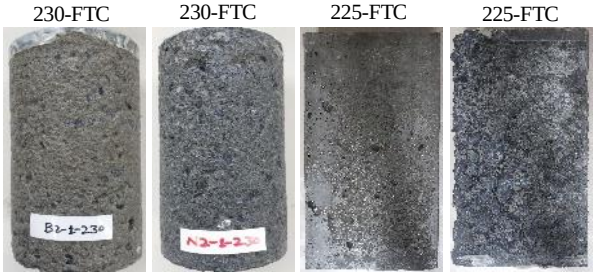

Fig. 8 Surface of F-T damaged concrete specimens

Fig. 7. It is found that the rate of reduction in RDEM with the increase in mass loss is slow for AE concrete regardless of compressive strength. However, the RDEM reduced rapidly with the mass loss for non-AE BFS concrete, which is because of internal micro-cracking induced by FTC due to absence of AE voids. The surface of frost damaged BFS concrete and normal concrete specimens at the end of 230-FTC in this study is shown in Fig. 8 along with 225-FTC damaged specimens of the previous study [1].

(2) Plastic strain growth

The strain variations with the change in temperature during freeze-thaw test in axial direction are shown in Fig. 9. The similar tendency was observed for strain variation in lateral direction. The plastic strain was increased with the increase in number of FTC. This is due to the reason that the hydraulic pressure is generated owing to expansion caused by freezing of water inside the pores of saturated concrete during freezing and thawing resulting in irreversible strain. This irreversible strain is accumulated with the increase in FTC number.

The FTC induced plastic strains for BFS concrete and normal concrete are shown in Fig. 10 both in axial direction and lateral direction. Due to high strength and provision of AE voids in both BFS and normal concrete, the cracking inside the concrete was prevented because of enough pores for expansion of ice; therefore, the rate of plastic strain development of AE concrete is almost similar and very small. Moreover, the development of plastic strain in axial direction for both concrete is found to be almost the same as that of lateral direction. The equivalent plastic strain due to FTC ($E_{p,ftc}$) is calculated from FTC induced plastic strain in axial and lateral by using Eq. (3) developed by Maekawa and Okamura

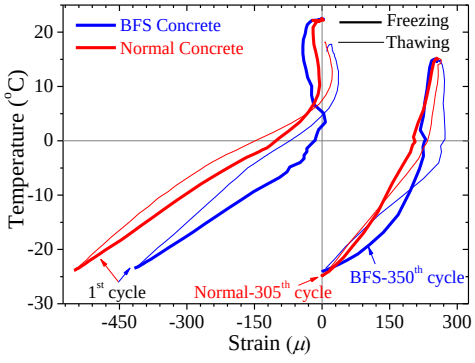

Fig. 9 Axial Strain variation during FTC

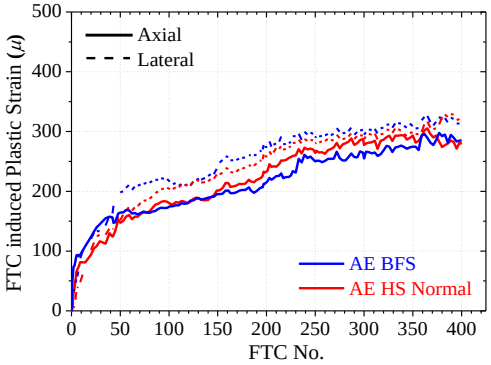

Fig. 10 FTC induced plastic strain

(1983) [13], as shown in Fig. 11. The actual peak strains at ultimate compressive strength obtained from uniaxial compression tests i.e. 2396μ for BFS concrete and 2562μ for normal concrete are used for the calculation of FTC equivalent plastic strain. The rate of increment of FTC equivalent plastic strain with the increase in FTC number is almost similar and very small for both concrete, which is due to provision of AE voids in the concrete. The similar tendency of $E_{p,ftc}$ increment for AE normal strength (NS) concrete with OPC as binder was observed by Hasan et. al. 2004 calculated using ε'_{co} of 2000μ [14] as shown in Fig. 11.

$$E_{p,ftc}=\sqrt{\left(\frac{0.31\sqrt{2}}{\varepsilon'_{co}}(\varepsilon_l+\varepsilon_a)\right)^2+\left(\frac{0.49\sqrt{2}}{\varepsilon'_{co}}(\varepsilon_l-\varepsilon_a)\right)^2} \quad (3)$$

Where,

ε'_{co} : peak strain at ultimate compressive strength

ε_l : FTC induced lateral strain

ε_a : FTC induced axial strain

3.2 Monotonic Behavior of Concrete

(1) Mechanical properties of concrete

The mechanical properties of intact specimens of both BFS concrete and HS normal concrete are presented

Table 2 Mechanical properties of AE BFS and AE HS normal concrete for 0-FTC

Type	f'_c (MPa)	E_c (GPa)	ε'_{c0} (μ)	v
BFS	61.3	34.8	2396	0.23
Normal	68.1	36.7	2562	0.22

f'_c: Ultimate compressive strength, E_c: Young's modulus, ε'_{co}: peak strain, v: Poisson's ratio.

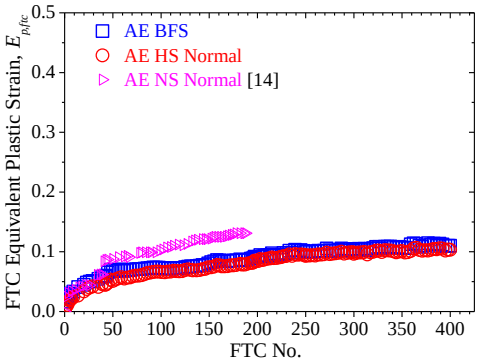

Fig. 11 Equivalent plastic strain due to FTC

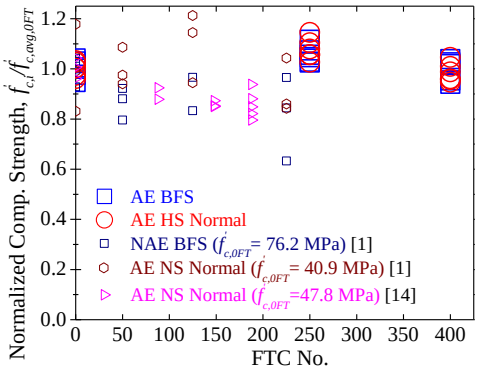

Fig. 12 Change in f'_c with FTC number

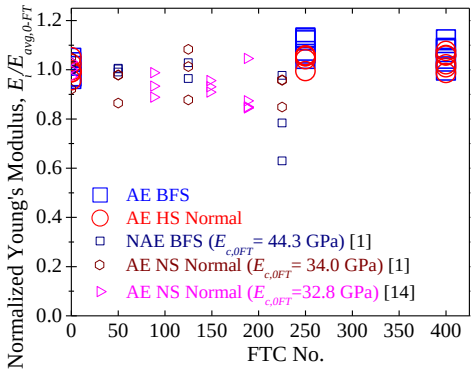

Fig. 13 Change in Young's Modulus with FTC No.

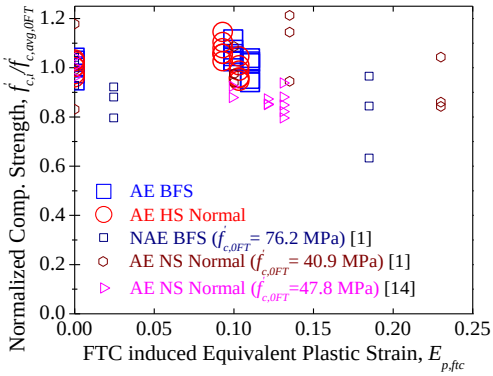

Fig. 14 Change in f'_c with $E_{p,ftc}$

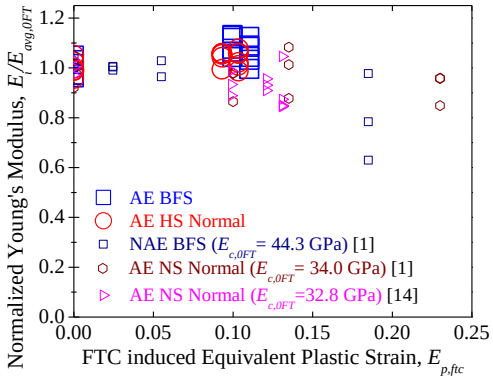

Fig. 15 Change in Young's Modulus with $E_{p,ftc}$

in Table 2. The values listed are the average of six specimens of each concrete. Normal concrete showed slightly better mechanical properties compared to BFS concrete. The change in mechanical properties i.e. compressive strength and Young's modulus for both BFS concrete and HS Normal concrete with the increase in number of FTC are shown in Figs. 12 and 13 respectively, and with equivalent plastic strain due to FTC ($E_{p,ftc}$) in Figs. 14 and 15 respectively, along with results from past studies [1, 14]. The values are normalized with the average f'_c and E_c at 0-FTC. The mechanical properties i.e. f'_c and E_c of AE BFS concrete and HS normal concrete did not degrade even after the application of 400-FTC, which might be because the amount and rate of equivalent plastic strain developed during FTC is very small owing to air-entrained voids and high strength of concrete. The other possible reason might be that the curing was resumed during FTC and it compensated the slight plastic damage caused by FTC. However, a slight degradation in mechanical properties for AE normal strength concrete was reported by Hasan et al. (2004) [14]. Moreover, the rate of degradation of mechanical properties for non-AE BFS [1] is more than that for AE BFS concrete.

(2) Fracture parameter change and plastic strain development

The fracture parameter (K) reduction and plastic strain development for AE BFS concrete and AE HS normal concrete for each frost damage level are shown in Figs. 16 and 17 respectively, along with for normal concrete proposed in elastoplastic and fracture (EPF) model [13] and for mortar [9]. No significant difference in fracture parameter change and plastic strain development for

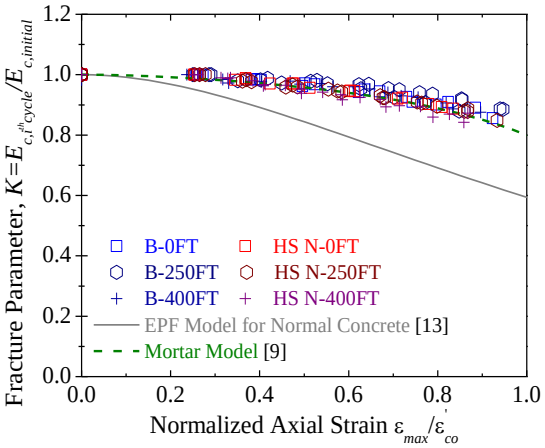

Fig. 16 Change in fracture parameter

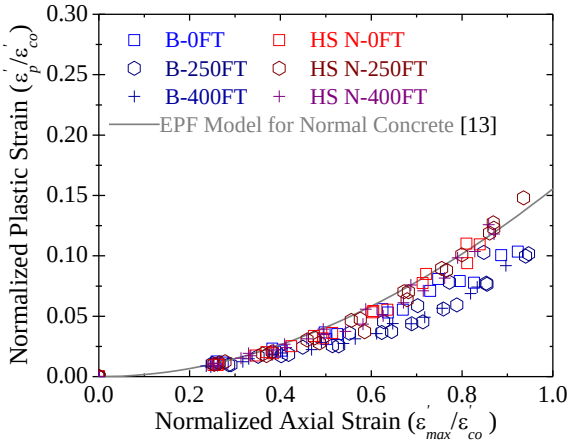

Fig. 17 Plastic strain development

different frost damage levels was observed. The fracture parameter for high strength concrete reduces slowly compared to that for normal concrete proposed in the EPF model. However, the fracture parameter change for high strength shows good agreement with the mortar model. Moreover, the plastic strain developed for HS normal concrete is almost the same as that for normal concrete proposed in EPF model [13]. However, it is slightly less for BFS concrete for each frost damage level.

The reason behind less reduction in fracture parameter and higher plastic strain development for HS concrete is that in the EPF model, the concrete is assumed as assembly for several constitutive microelements connected in parallel. Each micro element is composed of an elastic spring to account for internal stress mechanism and slider to consider the plastic deformation of concrete. Upon the application of load, some of the elements break resulting in plastic deformation and change in fracture parameter. The damage in concrete is modelled by fracture of elastic springs in micro-elements. For high strength concrete, it can be assumed that even the sliders show plastic deformation upon the application of load, the elastic springs are still active in taking the load. Therefore, the rate of change of fracture parameter for HS concrete is less than that for normal concrete in EPF model and plastic strain accumulation is almost the same.

4. CONCLUSIONS

This study was conducted to study the effect of freeze-thaw action on mechanical behavior of AE BFS concrete under static loading compared to AE high strength normal concrete. Following conclusions were drawn from this study:

(1) The rate of plastic strain development is almost similar and minimal for both BFS concrete and high strength normal concrete, which is due to air-entrained voids inside the concrete to accommodate the freezing of pore water and high strength of concrete.
(2) No significant reduction in compressive strength and Young's modulus for both BFS and normal concrete was observed even after 400-FTC, which is because of very small equivalent plastic strain induced due to FTC.
(3) Less rate of reduction in fracture parameter and comparatively more plastic strain development was observed for AE HS concrete, which might be because the elastic springs in constitutive microelements are still active in taking load while slider shows some plastic deformation upon the application of load.

ACKNOWLEDGEMENT

The authors would like to acknowledge the Council for Science, Technology and Innovation, ''Cross-ministerial Strategic Innovation Promotion Program (SIP), Infrastructure Maintenance, Renovation, and Management" (funding agency: NEDO) for supporting this research work.

REFERENCES

[1] Farooq, M. A. et al., "Mechanical Properties of Concrete with Blast Furnace Slag Fine Aggregates Subjected to Freeze-Thaw Cycles," in: High Tech Concrete: Where Technology and Engineering Meet, Springer, Cham., 2018, pp. 65-72
[2] Shi, S., "Effect of Freezing-Thawing Cycles on Mechanical Properties of Concrete," China Civil Engineering Journal, Vol. 30(4), 1997, pp. 35-42
[3] Valenza, J. J. and Scherer, G. W., "A review of salt scaling: II. Mechanisms," J. of Cement and Concrete Research, Vol. 37(7), 2007, pp. 1022-1034.
[4] Statistical Annual Report of Iron and Slag, Nippon Slag Association, Japan, 2011, pp. 2-3
[5] Jariyathitipong, P., "Improving the durability of concrete through the use of ground granulated blast furnace slag and blast furnace slag sand," PhD Dissertation, Okayama University, Japan, 2014
[6] Valcuende, M. et al. "Shrinkage of self-compacting concrete made with blast furnace slag as fine aggregate," J. of Construction and Building Materials, Vol. 76, 2015, pp. 1-9
[7] Murata, J. et al. "Resistance to Freezing and Thawing of Concrete Using Ground Blast-Furnace Slag," J. of Materials Div., ACI, Vol. 79, 1983, pp. 999-1012
[8] Ayano, T., and Fujii, T., "Resistance to Freezing and Thawing Attack of Concrete with Blast Furnace Slag Fine Aggregates," J. of Materials and Concrete Structures Div., JSCE, Vol. 70(4), 2014, pp. 417-427
[9] Farooq, M. A. et al. "Experimental and numerical investigation of static and fatigue behavior of mortar with blast furnace slag sand as fine aggregates in air and water," J. of Construction and Building Materials, Vol. 143, 2017, pp. 429-443
[10] ASTM C666–97, "Standard Test Method for Resistance of Concrete to Rapid Freezing and Thawing," ASTM, 1997
[11] ASTM C39/39-14, "Standard Test Method for Compressive Strength of Cylindrical Concrete Specimens," ASTM, 2014
[12] Ogata, H. et al. "Evaluation of Freezing and Thawing Characteristics of Concrete by Ultrasonic Method (Non-destructive Inspection and Diagnosis)," Proceedings of JCI, Vol. 24(1), 2002, pp. 1563-8
[13] Maekawa, K. and Okamura, H., "The deformational behavior and constitutive equation of concrete using the elasto-plastic and fracture model," J. of the Faculty of Engineering, University of Tokyo, Vol. XXXVII (2), 1983, pp. 253-328
[14] Hasan, M. et al., "Stress-Strain Model of Concrete Damaged by Freezing and Thawing Cycles," J. of Advanced Concrete Technology, Vol. 2(1), 2004, pp. 89-99